Available online at www.sciencedirect.com
ScienceDirect
Journal of Power Sources 178 (2008) 525–536
JOURNAL OF POWER SOURCES
www.elsevier.com/locate/jpowsour

Performance and degradation of high temperature polymer electrolyte fuel cell catalysts

A.S. Aricò *, A. Stassi, E. Modica, R. Ornelas, I. Gatto, E. Passalacqua, V. Antonucci

CNR-ITAE, Via Salita S. Lucia sopra Contesse 5, 98126 Messina, Italy

Received 12 July 2007; received in revised form 10 September 2007; accepted 2 October 2007
Available online 7 October 2007

Abstract

An investigation of carbon-supported Pt/C and PtCo/C catalysts was carried out with the aim to evaluate their stability under high temperature polymer electrolyte membrane fuel cell (PEMFC) operation. Carbon-supported nanosized Pt and PtCo particles with a mean particle size between 1.5 nm and 3 nm were prepared by using a colloidal route. A suitable degree of alloying was obtained for the PtCo catalyst by using a carbothermal reduction. The catalyst stability was investigated to understand the influence of carbon black corrosion, platinum dissolution and sintering in gas-fed sulphuric acid electrolyte half-cell at 75 °C and in PEMFC at 130 °C. Electrochemical active surface area and catalyst performance were determined in PEMFC at 80 °C and 130 °C. A maximum power density of about 700 mW cm^{-2} at 130 °C and 3 bar abs. O_2 pressure with 0.3 mg Pt cm^{-2} loading was achieved. The PtCo alloy showed a better stability than Pt in sulphuric acid after cycling; yet, the PtCo/C catalyst showed a degradation after the carbon corrosion test. The PtCo/C catalyst showed smaller sintering effects than Pt/C after accelerated degradation tests in PEMFC at 130 °C.

Keywords: PEMFCs; High temperature; Automotive; Pt catalysts; Pt alloys

1. Introduction

Recent advances in fuel cells technology demand operation at high working temperatures to improve efficiency, tolerance of contaminants and for an easy water management [1]. High temperature operation influences significantly carbon black corrosion, platinum dissolution and sintering [1–3]. Furthermore, a large-scale application of PEMFC systems technology requires a reduction of its high cost through a decrease of Pt loading and maximization of catalyst utilization as well as an improvement of performance and stability [3,4].

The catalysts employed in the present PEMFCs are mostly nanosized platinum particles supported on carbon; reduction of the noble metal content, enhanced catalytic activity and stability are significant challenges for this fuel cell technology on the way to become cost competitive.

High temperature PEMFC operation (130 °C) requires the development of catalysts with proper resilience to sintering and corrosion under working conditions. It is general opinion that corrosion resistant catalyst supports need to be selected for high temperature operation as well as proper anchoring of the metal phase on the support is necessary to improve stability [5–8]. Yet, no systematic study has been carried out to investigate the degradation properties of conventional fuel cell catalysts in PEM fuel cells under high temperature operation (e.g. 130 °C). This is mainly due to the scarce availability of polymer electrolyte membranes that can operate under such conditions. Since a wide number of research groups is actively involved in searching for high temperature solid polymer electrolytes [9–13], it appears appropriate to analyse the behaviour of catalysts under conditions similar to the target application for electro-traction [3]. Some information can be derived from corrosion studies carried out in phosphoric acid fuel cells using similar catalysts [14]. This is appropriate to evaluate the catalysts stability for phosphoric acid-doped polybenzoimidazole (PBI) fuel cell [15]; but it seems less useful for classical PEMFCs based on perfluorosulphonic membranes being the reaction environment quite different in these two fuel cell technologies.

The scope of this work is to evaluate the high temperature performance and stability of the catalysts in the presence of

* Corresponding author. Tel.: +39 090624237; fax: +39 090624247.
E-mail address: arico@itae.cnr.it (A.S. Aricò).

0378-7753/$ – see front matter © 2007 Elsevier B.V. All rights reserved.
doi:10.1016/j.jpowsour.2007.10.005

perfluorosulphonic membranes and to correlate these properties with the physico-chemical characteristics both in terms of electro-catalytic activity for oxygen reduction and resistance to degradation under fuel cell conditions. We have overcome the constraints related to the dehydration behaviour of the membrane at high temperature by pressurizing the PEM single cell and operating the humidifiers at the same temperature and pressure of the cell. Although, the operating conditions do not exactly reproduce those aimed by the automakers, i.e. ambient pressure and 25% relative humidity (RH) [3], the present approach may provide a basis to identify the high temperature degradation mechanism for conventional PEMFCs and alleviate through proper preparation procedures the performance loss.

Practical Pt/C anode and Pt/C or PtCo/C cathode catalysts with high metal surface area have been developed. Benchmark carbon blacks with intermediate and high surface area have been selected, i.e. Vulcan XC 72 with BET active area of 250 $m^2\ g^{-1}$ and Ketjenblack EC with BET active area of about 850 $m^2\ g^{-1}$. The synthesis process was optimised to obtain suitable dispersions of the metal particle sizes on the support even for high metal concentration catalysts (up to 50 wt.%) and a mean particle size smaller than 3 nm. The electrochemical studies have been focused on the oxygen reduction reaction being this process characterized by poor reaction kinetics compared to hydrogen oxidation. A small particle size is generally associated to a high active surface area necessary to increase the noble metal catalyst utilization; whereas, the reaction rate for oxygen reduction is not only associated to the dispersion but also to some structural characteristics that increase the specific activity of the catalysts. As well known from the literature [16–19], the crystallographic structure plays a significant role being the oxygen reduction a structure–sensitive process. Accordingly, our efforts were focused on the achievement of a proper crystalline structure with face-centered-cubic phase even for small particle size catalysts (1.5 nm). These materials have been characterized in terms of physico-chemical properties including structural (XRD), morphological (TEM) and elemental (CHNS-O and XRF) analyses. Electrochemical tests have been carried out in gas-fed sulphuric acid electrolyte half-cell at 75 °C and under PEM configuration at both 80 °C and 130 °C by using conventional thin perfluorosulphonic membranes.

2. Experimental

2.1. Catalyst preparation

A colloidal procedure to prepare Pt/C and PtCo/C catalysts with metal concentration ranging from 30 wt.% to 50 wt.% on different commercial carbon black supports was used [20]. Sulphite complexes of Pt, in appropriate amounts, were decomposed by hydrogen peroxide to form aqueous colloidal solutions of Pt oxides. These particles were adsorbed on carbon black. These first steps were carried out in CSTR reactors with digital stirring. Reactions were performed under proper pH and temperature operating conditions. The amorphous oxides on carbon were thus reduced in a hydrogen stream to form metallic particles. The step concerning Pt reduction was performed under controlled hydrogen stream with a continuous monitoring of gas consumption by a TCD. The PtCo/C catalyst was synthesized in a similar way. Before the reduction step, cobalt nitrate was adsorbed on the amorphous Pt/C catalyst. Both hydrogen and carbothermal reduction in inert (Ar) atmosphere were investigated for the preparation of carbon-supported PtCo alloy. The following catalysts were prepared:

- 30% Pt/Vulcan XC 72 via colloidal route followed by H_2 stream reduction (30% Pt/VC).
- 30% and 50% Pt/Ketjenblack EC via colloidal route followed by H_2 stream reduction (30% Pt/KB and 50% Pt/KB).
- 50% Pt–Co/Ketjenblack EC via colloidal route followed by H_2 stream reduction (50% Pt/KB H).
- 50% Pt–Co/Ketjenblack EC via colloidal route followed by carbothermal reduction at 500 °C (50% Pt/KB CA) and 600 °C (50% Pt/KB CB).

These catalysts were investigated as cathodes in all experiments. The 30% Pt/Vulcan XC 72 was used as anode in all PEM studies.

2.2. Physico-chemical analysis

The catalysts were characterized ex situ by different techniques. TEM analysis was made by first dispersing the catalyst powder in isopropyl alcohol. A few drops of these solutions were deposited on carbon film-coated Cu grids and analysed with a Philips CM12 microscope.

X-ray diffraction powder (XRD) patterns for these catalysts were obtained on a Philips X'Pert X-ray diffractometer using Cu Kα-source operating at 40 kV and 30 mA. The peak profiles of the (2 2 0) reflection in the face-centered-cubic (fcc) structure were obtained by using the Marquardt algorithm [20]. Instrumental broadening was determined by using a standard platinum sample. Electrodes were placed on a silicon substrate for XRD analysis. X-ray fluorescence analysis of the catalysts was carried out by a Bruker AXS S4 Explorer spectrometer operating at a power of 1 kW and equipped with a Rh X-ray source, a LiF 220 crystal analyser and a 0.12° divergence collimator. Quantitative analysis of light elements was carried out with Carlo Erba CHNSO instrument. SEM–EDX analyses of electrode–polymer electrolyte membrane interface were carried out by a FEI XL-30 FEG instrument.

2.3. Electrochemical studies

Electrodes and MEAs were prepared as reported in Ref. [21]. Electrochemical studies were carried out in both liquid electrolyte (sulphuric acid) gas-fed half-cell and in PEMFC. Half-cell studies served for preliminary evaluation and screening of catalysts; whereas, PEM studies at high temperature were carried out on the most promising formulations.

For operation in sulphuric acid-based half-cell and PEM single cell, hydrophobic backing layer and hydrophilic backing layers were used, respectively. This procedure was adopted to reduce the flooding effects in liquid electrolyte half-cell and

to enhance humidification at 130 °C in a PEMFC. The catalytic layer was prepared as for a standard PEMFC, i.e. 33 wt.% Nafion ionomer, 67 wt.% catalyst with Pt loading of 0.3 mg cm^{-2}.

An evaluation of catalyst stability was first carried out in a conventional thermostated three-electrode cell consisting of the gas-diffusion electrode to be tested (working electrode), a platinum grid (counter electrode) and a reference electrode (Hg/Hg_2SO_4 sat.). A gas was fed to the electrode backing layer during the experiments. The electrode area exposed to the liquid electrolyte was 0.5 cm^2.

The experiments to evaluate carbon and platinum stability were:

- Pt degradation test consisting in 1000 cycles between 0.6 V and 1.2 V RHE at 20 mV s^{-1}, in the presence of He feed in H_2SO_4 0.5 M.
- Chronoamperometry at 1.2 V RHE for 24 h, He feed, H_2SO_4 0.5 M.

The verification of the decay has been carried out "in situ" by:

- Conventional cyclic voltammetry in half-cell: H_2SO_4 0.5 M, 0.02–1.2 V RHE, He feed, 20 mV s^{-1}.
- Oxygen reduction polarizations in H_2SO_4 0.5 M at 75 °C, pure O_2 at atmospheric pressure.

Ohmic resistance was monitored during these experiments by ac-impedance spectroscopy (high frequency intercept on the real axis). Tafel plots were calculated after IR correction.

Membrane–electrode assemblies (MEAs) were formed by a hot-pressing procedure and subsequently installed in a fuel cell test fixture. This was connected to a fuel cell test station including an HP6060B electronic load and an AUTOLAB metrohm potentiostat/galvanostat equipped with a 20 A current booster. The humidifiers temperature was the same of cell temperature in all experiments. The cell temperature was measured by a thermocouple embedded in the cathodic graphite plate, close to the MEA. Electrochemical studies (polarization curves and ac-impedance) in PEMFC were performed in the presence of H_2–air and H_2–oxygen in a 5 cm^2 single cell at 80 °C (1 bar abs. and 3 bar abs.) and 130 °C (3 bar abs.) commercial Nafion 112 and 115 membranes with thickness of 50 μm and 100 μm (dry form), respectively were used. The oxygen and hydrogen flow rates were fixed at 2 and 1.5 times, respectively, the stoichiometry value corresponding to 1 A cm^{-2}. The Pt loading was 0.3 mg cm^{-2}. Single cell performances were investigated by steady-state galvanostatic measurements. For CV studies at 80 °C under PEMFC configuration, hydrogen (1 bar abs.) was fed to the anode that operated as both counter and reference electrode, whereas, nitrogen was fed to the working electrode. The sweep rate was 20 mV s^{-1}. The electrochemical active surface area was determined by integration of CV profile in the hydrogen adsorption region after correction for double layer capacitance. Data have not been corrected for hydrogen cross-over. Accelerated degradation tests in PEMFC were carried out at 130 °C by using the same configuration above described; both cell and humidifiers were pressurized and maintained at the same temperature. The accelerated tests for the cathode consisted in 1000 cycles between 0.6 V and 1.2 V RHE at 20 mV s^{-1}. After testing, the samples were characterized by "ex situ" physico-chemical analysis of catalytic layer to evaluate sintering and dissolution.

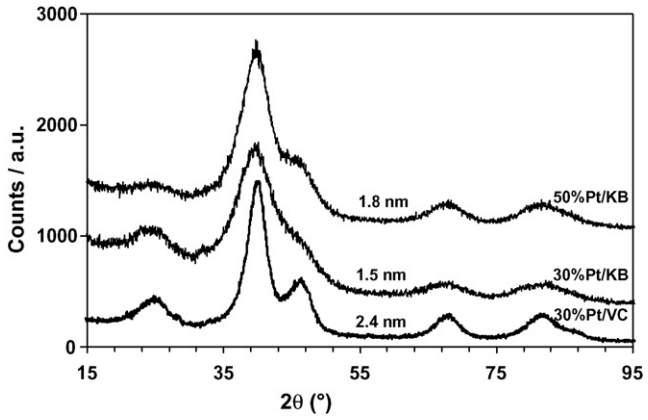

Fig. 1. XRD patterns of Pt catalysts supported on carbon blacks (Vulcan/VC vs. Ketjenblack/KB) with different concentrations (50 wt.% vs. 30 wt.%).

3. Results and discussion

3.1. Physico-chemical results

XRD patterns and TEM micrographs of Pt/C and Pt_3Co_1/C catalysts are reported in Figs. 1–4, respectively. X-ray fluorescence and CHNSO elemental analysis confirmed the nominal compositions. For the Pt/C catalysts, the carbon black support and concentration of metal phase on carbon were varied. For the PtCo/C series, concentration of metals and carbon black support

Table 1
Catalyst properties

Catalyst	Peak pos. 220/(2θ)	A_0 (nm)	Mean particle size (nm)	Atomic ratio Pt/Co (XRF)	ECSA[a] (m^2 g^{-1})
30% Pt/VC	67.710	0.391	2.4	–	51
30% Pt/KB	67.549	0.392	1.5	–	120
50% Pt/KB	67.645	0.392	1.8	–	72
50% Pt_3Co_1/KB H	68.113	0.389	1.7	3.08	–
50% Pt_3Co_1/KB CA	68.450	0.388	2.5	2.88	–
50% Pt_3Co_1/KB CB	69.059	0.385	2.9	2.89	44

[a] Determined in PEMFC at 80 °C.

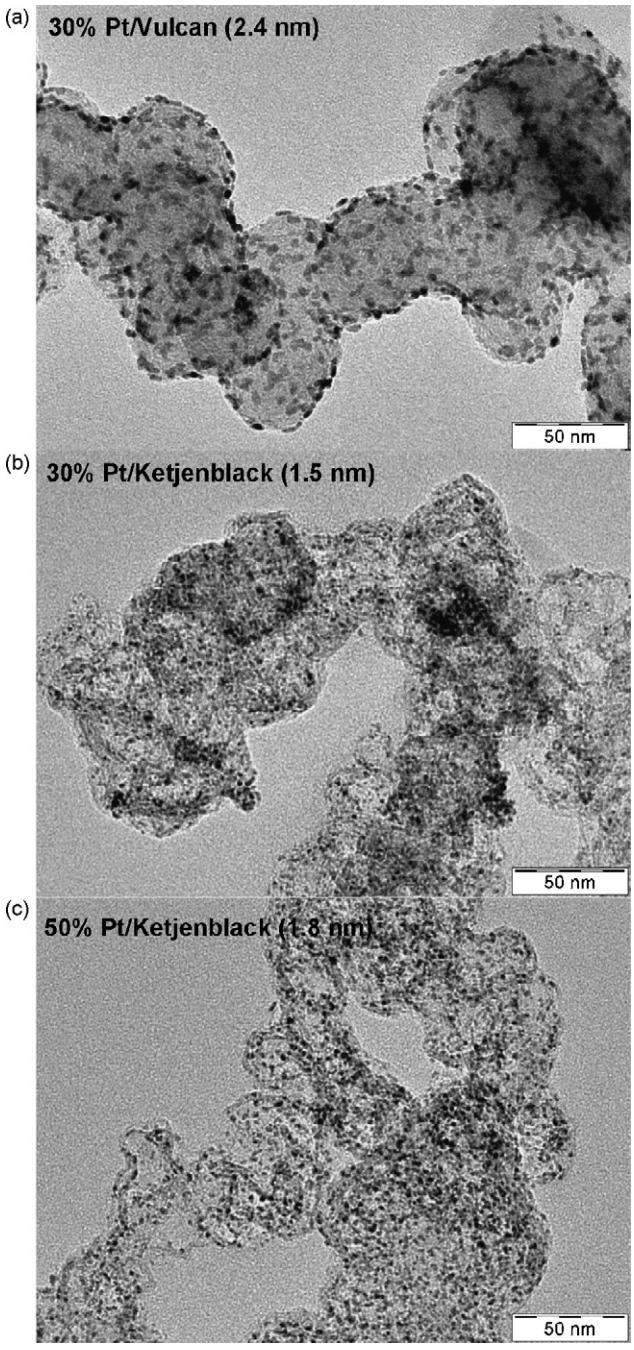

Fig. 2. TEM micrographs of different carbon-supported Pt catalysts.

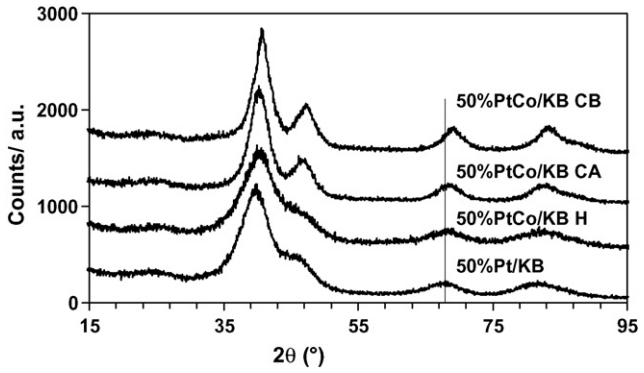

Fig. 3. XRD patterns of 50% Pt–Co catalysts supported on Ketjenblack (Pt_3Co).

were maintained constant; whereas, the reduction treatment was varied. The high surface area carbon black was selected for the Pt–Co series to enhance the dispersion since the catalysts were treated at high temperature.

The catalysts showed cubic structure for Pt and PtCo (fcc) and hexagonal structure for carbon support. Both XRD and TEM analyses indicated a small particle size ranging from 1.5 nm to 3 nm with unimodal distribution. A good dispersion was obtained for all catalysts. The lattice parameter (A_0), the mean particle size, derived from XRD, and Pt/Co atomic ratio, derived from XRF, are reported in Table 1. For Pt/C catalysts, the particle size increased as a function of the increase of metal phase concentration and the decrease of BET surface area of carbon support. For PtCo/C catalysts a large lattice contraction corresponding to high degree of alloying was achieved only after a high temperature treatment (600 °C). This determined an increase of the particle size to 2.9 nm with a loss of metal surface area (Table 1). A 20% amount of Co atomic concentration in the PtCo fcc structure was calculated from the Vergard's law for the 50% PtCo/KB CB catalyst.

3.2. Catalytic activity and degradation tests in sulphuric acid

Fig. 5 summarizes the catalytic activity for oxygen reduction in half-cell at 75 °C in 0.5 M H_2SO_4, with pure oxygen feed. The catalyst with a mean particle size of 2.4 nm (30% Pt/VC) showed the best performance in the activation-controlled region. In the Tafel region, the performance increased as a function of the particle size in the investigated range. The Tafel slope was about 70 mV dec^{-1} for all catalysts indicating a similar reduction mechanism.

We have focused our attention on small particle size catalysts characterized by a strong metal support interaction [8]. It is well known that increasing the mean particle size, the mass activity for oxygen reduction passes through a maximum and then decreases [16]. The particle size of these catalysts falls in the left region of the Kinoshita volcano-shape curve of mass activity vs. particle size [16].

Different accelerated test procedures have been selected to evaluate catalyst stability [3]; these are preliminarily discussed below:

- Evaluation of Pt sintering by continuous cycling between 0.6 V and 1.2 V vs. RHE, i.e. in the region where Pt is less stable. It is known that the formation of a stable Pt-oxide phase at potentials higher than 1.2 V RHE stabilizes Pt; whereas, at potentials smaller than 0.6 V RHE the corrosion effects are negligible.
- Evaluation of carbon corrosion on the deposited Pt nanosized particles by holding a constant potential of 1.2 V RHE for 24 h, in an electrochemical gas-fed half-cell. At high electrochemical potentials, carbon corrosion with consequent CO_2 formation is greatly accelerated.

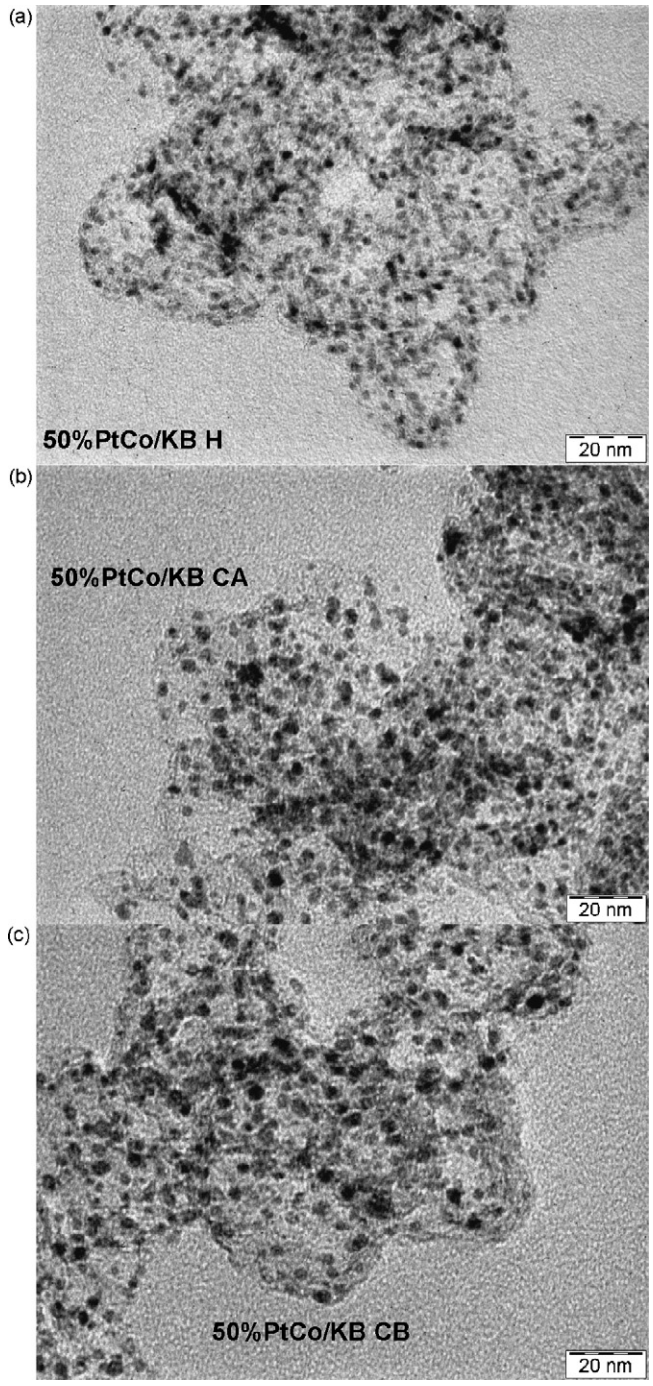

Fig. 4. TEM micrographs of 50% Pt–Co catalysts supported on Ketjenblack (Pt_3Co).

Pt degradation test has been done by carrying out 1000 cycles between 0.6 V and 1.2 V RHE at 20 mV s^{-1} with He feed in 0.5 M H_2SO_4. In Fig. 6, some cycles, registered during this test for 30% Pt/Vulcan, are shown. It was clearly observed that the PtO reduction peak shifted to high potentials and decreased in intensity. These effects were attributed to an increase of specific activity for the oxygen reduction reaction due to the increase of particle size (sintering) and a reduction of the electrochemically active surface area (ECSA), respectively. Both aspects determine the mass activity for the oxygen reduction process

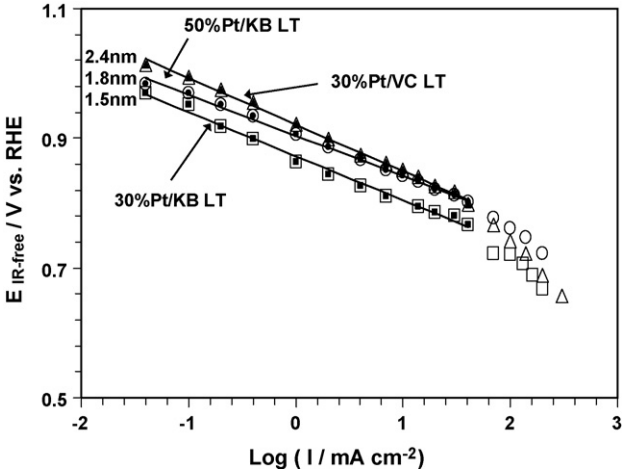

Fig. 5. Effect of particle size on the Tafel plots for oxygen reduction at the Pt/C catalysts in sulphuric acid: 0.5 M H_2SO_4; 75 °C, pure O_2. Flooded conditions.

[16]. A modification of the catalyst properties occurs during the accelerated tests as a consequence of the Pt dissolution reprecipitation process (particle growth) [22]. The peak potential for PtO reduction is determined by the difference of the chemical potential of the Pt–O and bare Pt, as well as by the activity of Pt–O and Pt. It has been shown in the literature that the peak potential of PtO reduction is related to the intrinsic catalytic activity for the oxygen reduction process [3]. A shift of the PtO reduction peak to higher potentials reflects a decrease of the adsorption strength for the oxygen containing species on the surface, e.g. OHads, which are believed to reduce the oxygen reduction activity [23–26]. Thus, such shift is associated to an increase of specific activity for oxygen reduction [3]. The latter increases as the particle size increases [1 1 7], as it usually occurs in a Pt sintering process. The CV profile after the Pt degradation test also shows an increase of the double layer capacitance (Fig. 7). Generally, such effect is interpreted in the literature as due to an increase of functional groups on carbon black support [27,28] due to the occurrence of carbon surface modification. The active area reduction after the Pt corrosion test for the 30% Pt/VC can be observed in Fig. 7. The ECSA decreased of about

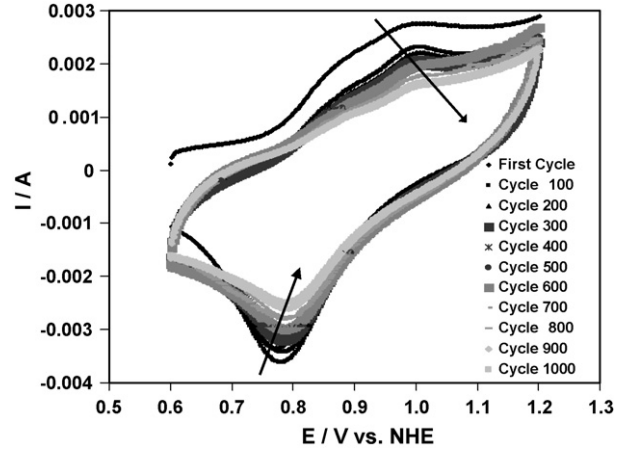

Fig. 6. Accelerated Pt degradation tests for 30% Pt/VC: 1000 cycles at 75 °C in 0.5 M H_2SO_4.

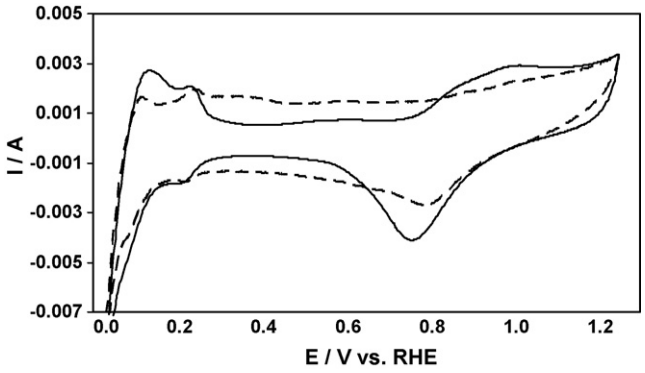

Fig. 7. Cyclic voltammetries of 30% Pt/VC electrode before (full line) and after (broken line) Pt degradation test (20 mV s^{-1}, 75 °C, 0.5 M H_2SO_4).

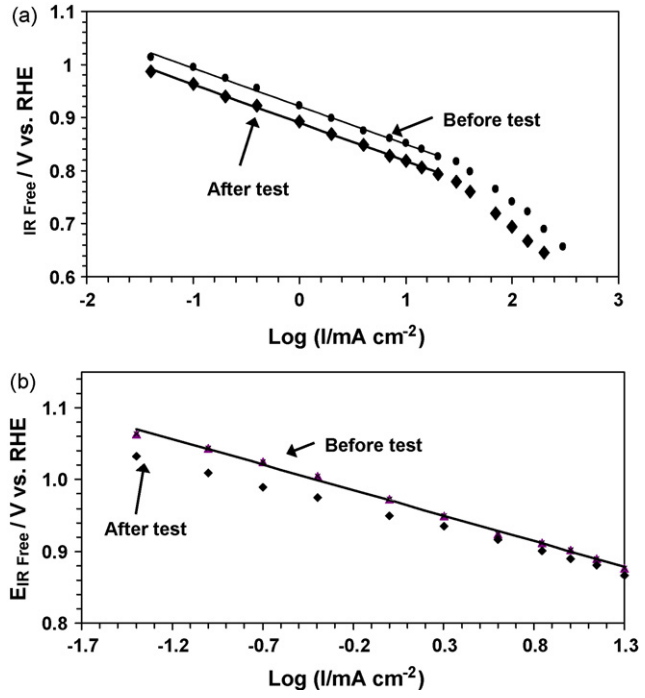

Fig. 8. Effect of electrode cycling (a) and potential holding at 1.2 V for 24 h (b) on the polarization behaviour for oxygen reduction of the 30% Pt/VC electrode. Pt loading 0.3 mg cm^{-2}; 0.5 M H_2SO_4; 75 °C, pure O_2.

50%. The effect of potential cycling (Pt degradation test) on electrode performance of 30% Pt/VC is illustrated in Fig. 8a. An average loss of 32 mV in the Tafel region was observed; no significant mass transport losses were recorded at high current density after the degradation test. The effect of electrode potential holding at 1.2 V (carbon corrosion test) on the performance

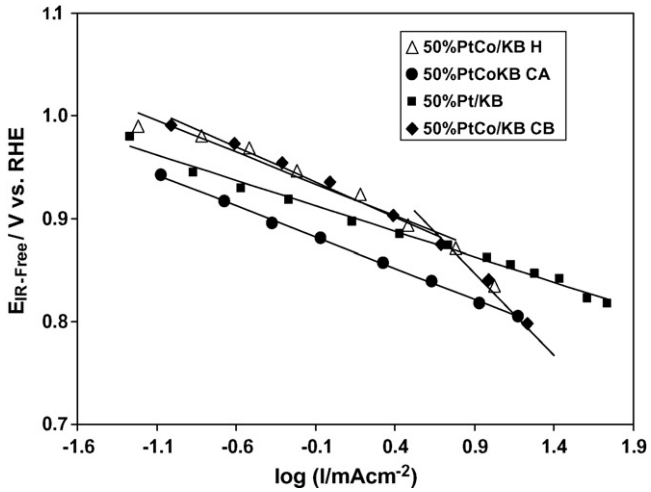

Fig. 9. Oxygen reduction Tafel plots for Ketjenblack supported 50% Pt_3Co_1 and Pt catalysts. Pt loading 0.3 mg cm^{-2}; 0.5 cm^2; 0.5 M H_2SO_4; 75 °C, pure O_2.

is shown in Fig. 8b; an average loss of about 23 mV in the Tafel region was recorded (Table 2).

Similar effects were observed for 30% and 50% Pt/KB catalysts. Data concerning with degradation tests in sulphuric acid half-cell are summarized in Table 2. Accordingly, in sulphuric acid half-cell, the Pt/VC catalyst appeared to be more stable than Pt/KB catalysts; this is possibly due to the smaller surface area of the Vulcan carbon support compared to Ketjenblack and the different particle size.

No significant effect was envisaged for the metal loading; whereas, a poor stability was observed in the presence of a catalyst with small particle size (Table 2). Large Pt particle size and a small carbon black surface area appear to enhance the stability in sulphuric acid in agreement to what has been observed in PAFCs [22,29]. It was observed in this catalyst series (Pt/C) that the accelerated Pt degradation test (potential cycling) caused a larger degradation of performance than the accelerated carbon corrosion test (oxidation at 1.2 V). The final particle size, in the Pt/C catalyst series, after the accelerated tests appeared to be determined by both degradation (sintering) occurring during the experiment and initial particle size (see Tables 1 and 2). As example, the final particle size of the 30% Pt/KB catalyst, characterized by high dispersion, was the smallest among the Pt/C series although a significant electrochemical degradation was registered for this catalyst. Thus, besides sintering, other phenomena (dissolution) may contribute to the performance loss.

Kinetic studies were also carried out for PtCo catalysts (Fig. 9). The Tafel plots show that, at low current densities, the

Table 2
Catalyst degradation in sulphuric acid half-cell

Catalyst	Potential loss after electrode cycling (mV)	Potential loss after carbon corrosion test (mV)	Particle size after electrode cycling (nm)	Particle size after carbon corrosion test (nm)
30% Pt/VC	32	23	8.4	4.2
30% Pt/KB	47	42	6.4	2.9
50% Pt/KB	39	36	7.0	3.4
50% PtCo/KB CB	≈0	50	5.0	7.0

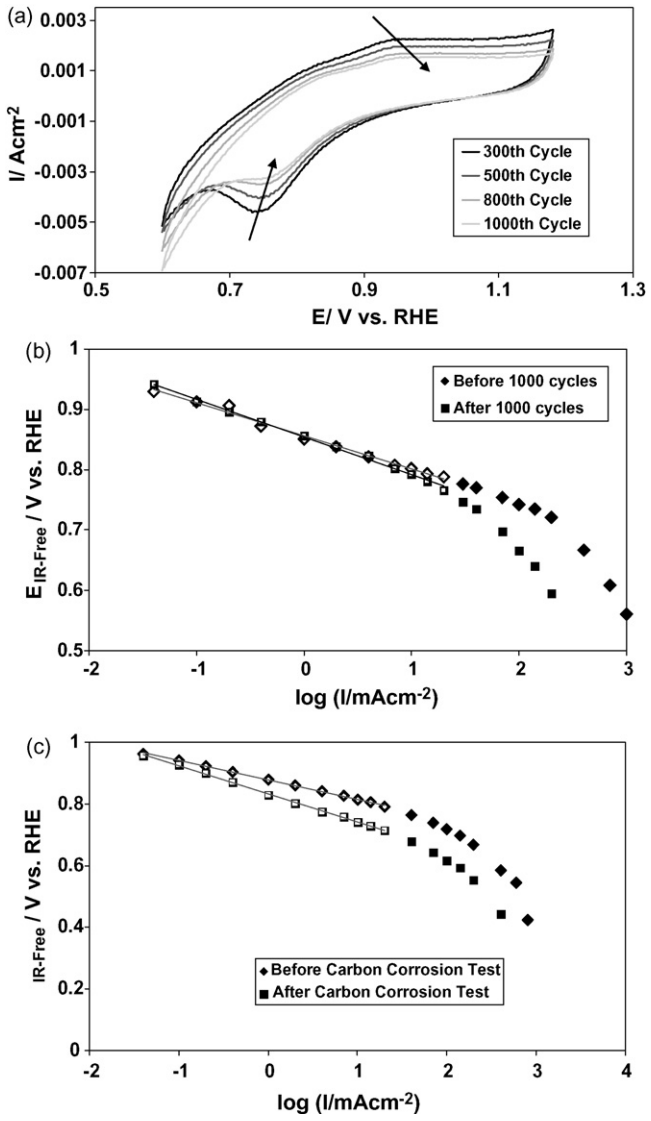

Fig. 10. Accelerated degradation: (a) 1000 cycles at 75 °C in 0.5 M H_2SO_4; effect of potential cycling (b) and potential holding at 1.2 V for 24 h (c) on the polarization behaviour of 50% PtCo/KB CB; Pt loading 0.3 mg cm^{-2}; 0.5 M H_2SO_4; 75 °C, pure O_2.

best performance was achieved with the PtCo catalyst characterized by high degree of alloying and large particle size (2.9 nm). The performance of PtCo catalysts did not show any correlation with the particle size as opposite of Pt/C catalysts. This may be due to the different reduction procedure used for the various PtCo catalysts, possibly, causing a different surface concentration of Pt and Co. A Tafel slope of about 60 mV dec^{-1} was observed for the PtCo series. A doubling of Tafel slope and a decrease of catalytic activity was envisaged at high current densities for some of the PtCo/C catalysts. However, in this region mass transport properties and flooding effects may affect the electrochemical behaviour. Thus, it is difficult to assign these effects to catalytic properties only.

The results related to the degradation behaviour of the most promising PtCo catalyst (50% PtCo/KB CB) are reported in Fig. 10a–c and in Table 2. Electrode cycling also caused for the PtCo catalyst a shift of the oxide reduction peak to high potentials and a reduction in current density (Fig. 10a). These effects are associated to an increase of the intrinsic activity and a decrease of the surface area with time as previously observed for Pt/C catalysts. The effects of potential cycling and potential holding at 1.2 V on the performance are illustrated in Fig. 10b and c, respectively. It is observed that the carbon corrosion plays a more important effect than the PtCo degradation (electrode cycling) on the stability of PtCo/C catalyst on the contrary of Pt/C catalysts (Table 2). It has been observed in the literature that the PtCo alloy is more stable than pure Pt during electrochemical tests [27,30,31]. In any case, a small Co dissolution occurs during electrochemical operation [3,19]; this increases the surface roughness, thus, limiting the effect of electrochemical sintering. The role of the carbon support on the catalyst degradation behaviour has been also emphasized [27]. Our separate degradation tests (electrode cycling and potential holding at 1.2 V RHE) indicate that the effect of the carbon support on the degradation is predominant; thus, most of the efforts should be concentrated on this aspect. In this regard, it should be mentioned that important progress has been made in the literature in the last years [6,32,33]. The increased stability of PtCo alloy vs. Pt in the Tafel region probably modifies the degradation process of the bimetallic catalyst with respect to the carbon-supported platinum. Colón-Mercado and Popov [31] individuated particle migration for pure Pt and Ostwald ripening for PtCo as the main degradation mechanisms. A potential loss for the PtCo catalyst is also observed in the mass transport controlled region, after potential cycling (Fig. 10b); however, this effect may be due to electrode flooding with time. These results are confirmed by XRD analysis. An increase of particle size from 3 nm to 5 nm and 7 nm for PtCo is observed after potential cycling (Pt degradation) and potential holding at 1.2 V (C corrosion), respectively (Fig. 11, Table 2). A partial dealloying occurs during Pt and carbon degradation tests as revealed by a shift in the fcc structure diffraction peaks to low Bragg angles (Fig. 11).

3.3. PEMFC studies

It was observed in the sulphuric acid half-cell studies that among the Pt/C catalysts, the 30% Pt/VC showed the best characteristics in terms of stability and catalytic activity. The behaviour of 30% Pt/VC catalyst was thus investigated in a PEMFC with hydrogen–air feed at 80 °C and 130 °C (3 bar abs.) in the presence of commercial thin Nafion 112 membrane

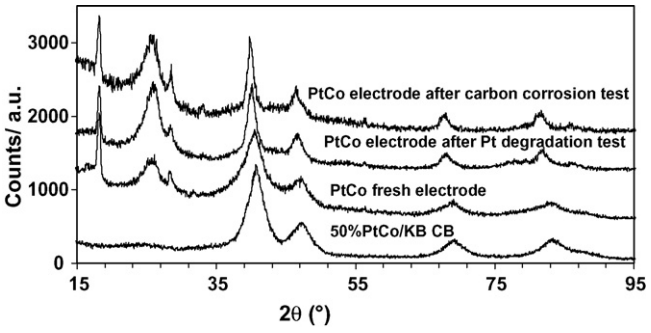

Fig. 11. XRD diffraction for PtCo after Pt and C degradation tests.

(50 μm). The catalyst stability was first investigated by operating the PEMFC for 24 h at a constant voltage of 0.7 V and 130 °C. During these experiments the PEM single cell was pressurized at 3 bar abs. and RH was 100%. The performances in single cell PEMFC at 80 °C (Fig. 12a) and 130 °C (Fig. 12b) are reported before and after this time test at 130 °C (not shown). It was observed a decrease of OCV and performance passing from 80 °C to 130 °C. The decrease of OCV is related to the increase in membrane swelling at 130 °C; this usually causes an increase of the hydrogen cross-over through the electrolyte and, thus, a mixed potential at the cathode. The increase of hydrogen cross-over with the temperature has been previously reported [34]. It should be also mentioned that this temperature is larger than the glass transition temperature of Nafion. The decrease of OCV is also observed at 80 °C after operation at 130 °C. A smaller limiting current density was recorded at 130 °C than at 80 °C. ac-Impedance spectroscopy analysis (Fig. 13a and b) did not reveal a significant increase in resistance if proper pressure and humidification conditions were selected at 130 °C. The average series resistance increased from 0.16 Ω cm^{-2} to 0.18 Ω cm^{-2} as the temperature increased from 80 °C to 130 °C. On the other hand, a significant increase of the charge transfer resistance at 130 °C with respect to 80 °C was recorded even at high cell potentials where mass transport is not a limiting step. This indicates an increase of the overpotential for the oxygen reduction process that is possibly related to a decrease of oxygen solubility at the electrode–electrolyte interface as the temperature is increased. The kinetic results in sulphuric acid half-cell are compared to PEM single cell data (Fig. 14) for the 30% Pt/VC. A similar Tafel slope is observed at low temperature indicating a similar mechanism. Unfortunately, at high temperature the effect of hydrogen cross-over limits significantly the catalytic activity of the electrode close to 0.9 V in the PEM single cell and it also causes a modification of the slope (Fig. 14).

In order to reduce the effects of cross-over, a thicker membrane, i.e. Nafion 115 (100 μm), was selected. It was observed an increase of OCV but also a significant increase of the ohmic

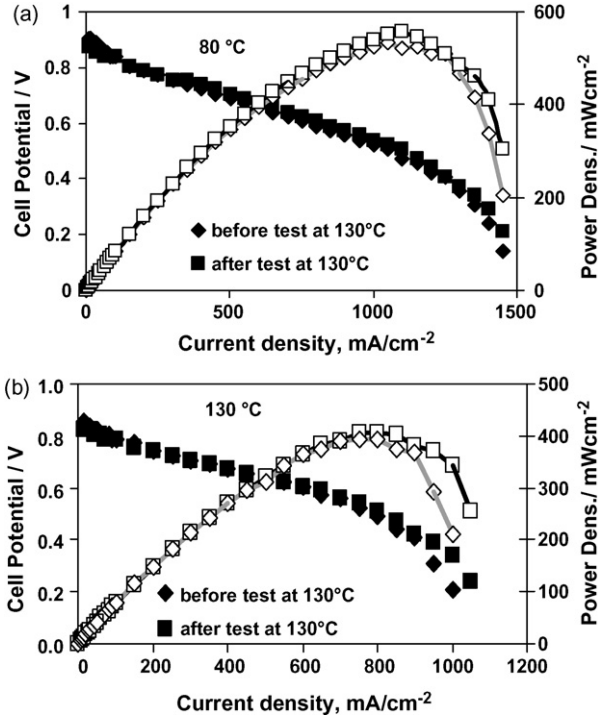

Fig. 12. Polarization and power density curves at 80 °C (a) and 130 °C (b) for a MEA based on 30% Pt/VC, in the presence of N112 membrane, before and after operation at 130 °C for 24 h. Cathode: air feed, 3 bar abs.

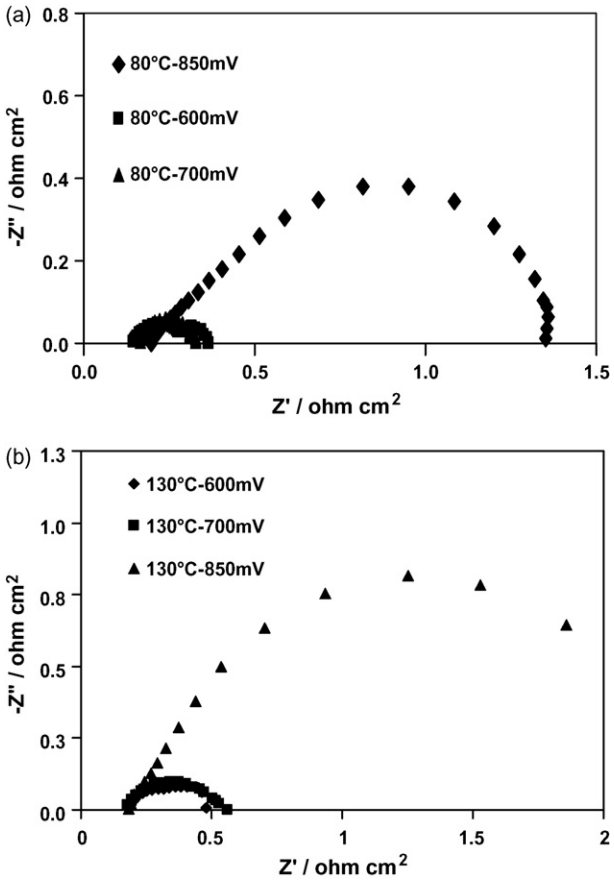

Fig. 13. Electrochemical impedance spectra collected during operation at 80 °C (a) and 130 °C (b) for a MEA based on 30% Pt/VC, in the presence of N112 membrane. Cathode: air feed, 3 bar abs.

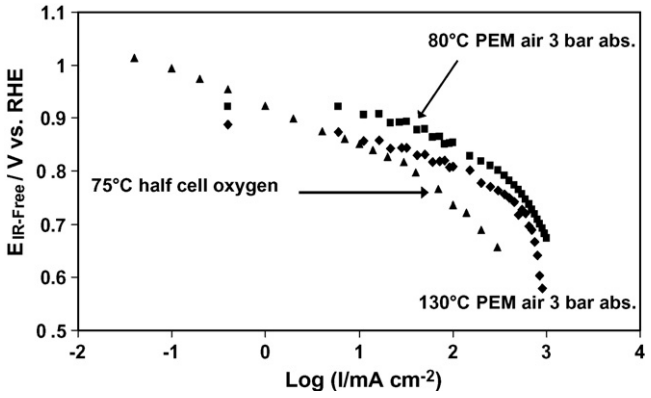

Fig. 14. Comparison of IR-free polarization curves for oxygen reduction in sulphuric acid half-cell and PEMFC for the 30% Pt/VC catalyst. Conditions are indicated in the figure.

resistance especially at 130 °C (not shown) due to humidification constraints.

By comparing at 80 °C the polarization behaviour of the Pt/C catalysts before and after operation at 130 °C for 24 h with Nafion 115, it was observed that the performance before high temperature operation followed a trend similar to that recorded in sulphuric acid in half-cell. Interestingly, after operation at 130 °C, the 50% Pt/ KB catalyst increased its performance and surpassed that of 30% Pt/VC (Fig. 15). The latter showed a slight decrease of activity that was not previously observed with the thin membrane. These results were interpreted on the basis of electrochemical active surface area (ECSA) changes after high temperature operation (Fig. 16a–c). The CV profiles showed a shift of the Pt-oxide reduction peak towards high potentials and a positive slope as a function of the potential in the double layer region. The latter indicates the presence of strong hydrogen cross-over (no diluted hydrogen was used at the anode/counter electrode).

The ECSA decreased from 51 $m^2\,g^{-1}$ to 39 $m^2\,g^{-1}$ for 30% Pt/VC after 130 °C operation; a decrease from 72 $m^2\,g^{-1}$ to 51 $m^2\,g^{-1}$ was observed for 50% Pt/KB; a shift of the peak potential for Pt-oxide reduction to high potentials indicated an increase in specific activity for oxygen reduction, as previously discussed, after operation at 130 °C due to Pt sintering. A modification in the CV profile of the 30% Pt/VC was also observed after operation at 130 °C. But, due to the very small particle size of this catalyst, the final ECSA was high, i.e. about 115 $m^2\,g^{-1}$. Possibly, the best compromise for this series of catalysts (Pt/C) in terms of specific activity for oxygen reduction and number of Pt sites available for the reaction corresponds to an ECSA value close to 50 $m^2\,g^{-1}$ [16,17]. Thus, this explains why the performance of the 50% Pt/KB increases when the surface area decreases from 72 $m^2\,g^{-1}$ to 51 $m^2\,g^{-1}$. Such analysis also explains why the performance of the 30% Pt/KB is poor. This is the consequence of low specific activity for a very high surface area catalyst. It is pointed out that such analysis concerns with catalysts that have operated for a short time at 130 °C (24 h) and it does not include the effect of Pt dissolution that occurs after prolonged operation and/or after specific accelerated degradation tests (see below). Furthermore, all data were not corrected for hydrogen cross-over; thus, the absolute value of the ECSA for these catalysts may be slightly different from

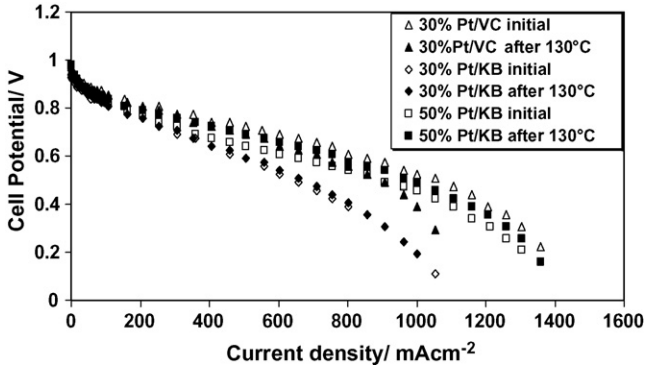

Fig. 15. Comparison of the polarization bevaviour for the various catalysts in the presence of Nafion 115 membrane before and after operation at 130 °C.

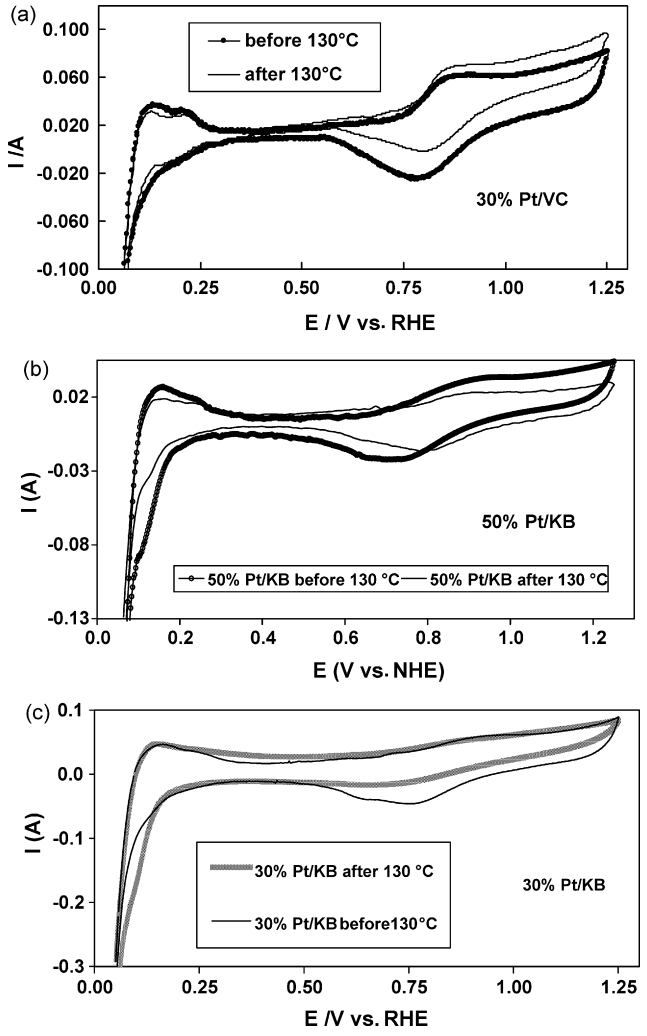

Fig. 16. Comparison of the CV profiles (20 mV s^{-1}) for the 30% Pt/VC (a), 50% Pt/KB (b) and 30% Pt/KB (c) catalysts, in the presence of Nafion 115 membrane before and after operation at 130 °C.

those estimated. For carbon-supported catalysts, mass activities slightly better than 100 A g^{-1} under air feed operation and without correction for hydrogen cross-over were recorded at 130 °C, 0.9 V RHE for 30% Pt/VC and 50% Pt/KB before and after operation at 130 °C, respectively. These activities are close to the benchmark PEMFC Pt/C catalysts at 80 °C [3].

On the contrary of sulphuric acid half-cell, accelerated Pt degradation tests carried out in PEM single cells at 130 °C showed that the Pt/KB was more stable than Pt/VC with respect to sintering by using the same cycling procedure. This was confirmed by both XRD and TEM analyses. As an example, XRD patterns of the cathodes before and after 1000 cycles at 130 °C between 0.6 V and 1.2 V (Fig. 17), showed slightly larger sintering for 30% Pt/VC than 50 % Pt/KB (particle size 12 nm vs. 8 nm). The lower degradation of the 50% Pt/KB catalyst with respect to the 30% Pt/VC catalysts is probably associated to the high surface graphicity index of Ketjenblack and anchoring effect of Pt particles to the support surface as a consequence of a better metal–support interaction [8]. It is derived that the corrosion mechanisms in sulphuric acid liquid electrolyte and

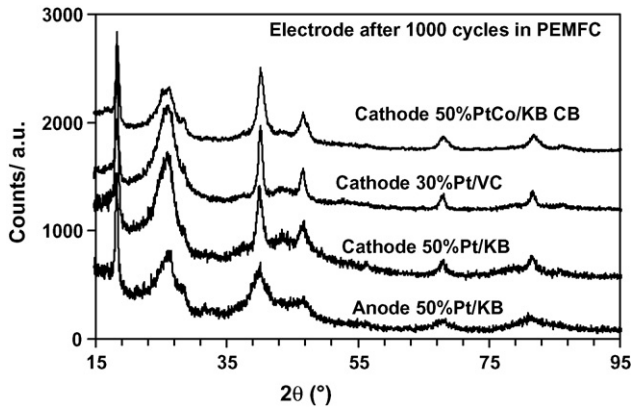

Fig. 17. X-ray diffraction patterns of the Pt/C and PtCo/C catalysts after a Pt degradation test of 1000 cycles between 0.6 V and 1.2 V vs. RHE in PEMFC at 130 °C.

in PEMFC (130 °C) are not exactly the same [22]. These effects were confirmed by the investigation of the membrane–electrode interface after potential cycling at 130 °C (Fig. 18). It was observed a significant dissolution and growth of Pt particles in the membrane for 30 % Pt/VC compared to 50 % Pt/KB. In the latter case, observation at large magnification indicated a much smaller amount of Pt particles in the membrane. Similar dissolution of Pt particles and precipitation inside the membrane has been also reported in the literature after a time study at 80 °C [35]. It is derived that the potential cycling procedure used here effectively represents an accelerated degradation test.

The performances of 50% Pt/KB and 50% PtCo/KB catalysts were compared in the presence of Nafion 112 membrane at 80 °C at low pressure, i.e. 1 bar abs. O_2, and at 130 °C with high pressure, i.e. 3 bar abs. O_2 (Fig. 19a and b). Oxygen feed was preferred in these tests to counteract the effects of cross-over that may alter the comparison. The performance of 50% PtCo/KB slightly increased passing from 80 °C to 130 °C as opposite of 50% Pt/KB. In the latter case, the performance did not vary significantly with the temperature. Whereas, it was shown above that the performance of the 30% Pt/VC decreased with the temperature. The increase of power density with the temperature for PtCo is possibly associated to surface modifications occurring upon high temperature operation. It should be mentioned that the PtCo catalyst was not pre-leached. Another aspect concerns with the hydrophilic nature of hydrous oxides formed on the base–metal surface of the Pt-alloy catalyst [3] that may enhance the hydration properties at high temperature. All these aspects will be investigated more in-depth in a next work.

The XRD patterns of Pt/KB and Pt/VC catalysts after 1000 cycles at 130 °C between 0.6 V and 1.2 V were already compared in Fig. 17. This figure also shows the pattern of 50% PtCo/KB CB catalyst after the same degradation test. The better stability of 50% PtCo/KB CB catalyst over Pt/C catalysts, observed in sulphuric acid after potential cycling, was confirmed by these PEM studies at 130 °C. The final particle size of 50% PtCo/KB CB after 1000 cycles at 130 °C was 6 nm as compared to 8 nm and 12 nm for 50% Pt/KB and 30% Pt/VC, respectively. The better stability of PtCo vs. pure Pt, observed by various authors in PEMFCs at low temperatures, e.g. 80 °C [27,30,31], is practically confirmed at 130 °C. The two different degradation processes, i.e. particle migration for Pt and Ostwald ripening for PtCo, envisaged at low temperature [31] may also govern the corrosion behaviour of these catalysts at 130 °C. It was reported that, in the case of Pt catalysts, crystallites which

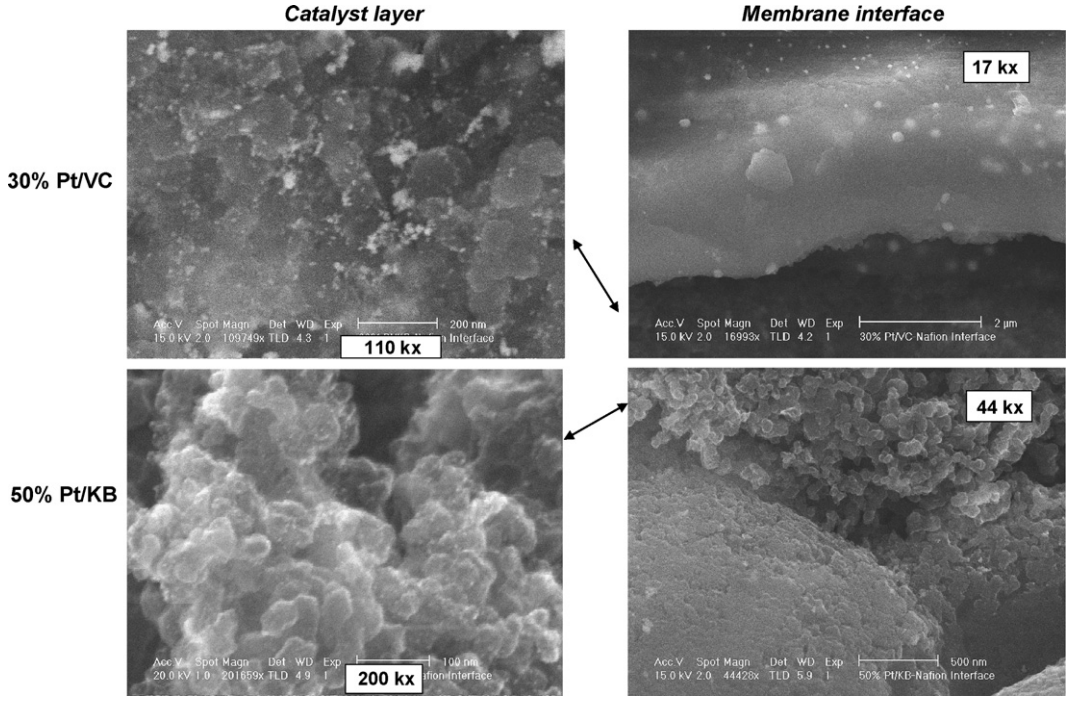

Fig. 18. SEM micrographs of cathode layer and cathode/membrane electrolyte interface for 30% Pt/VC and 50% Pt/KB catalysts after a degradation test of 1000 cycles between 0.6 and 1.2 V vs. RHE in PEMFC at 130 °C. The magnification of the interface is larger for 50% Pt/KB than 30% Pt/VC.

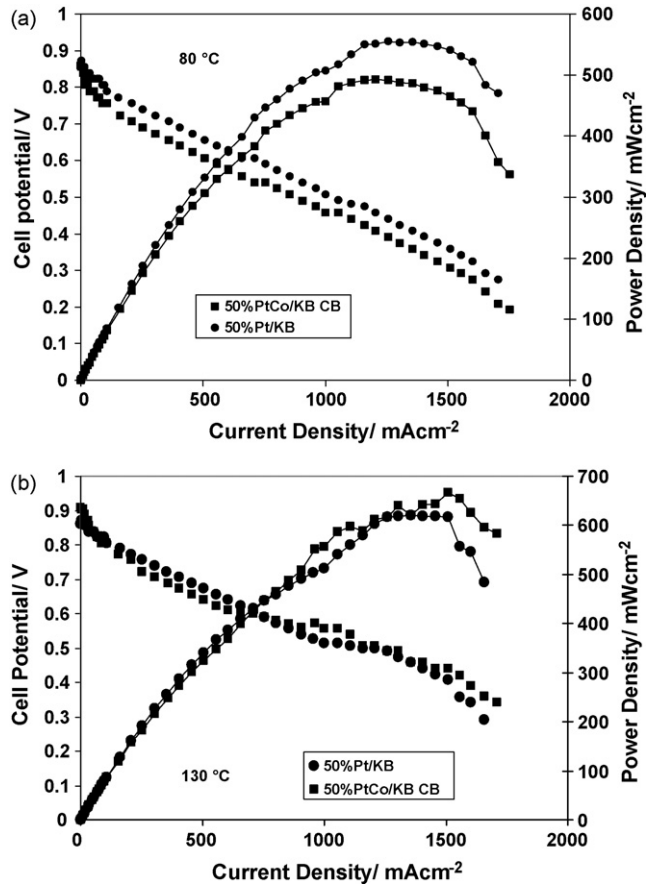

Fig. 19. PEMFC polarization curves for Pt/C and PtCo/C catalysts in the presence of Nafion 112 membrane at 80 °C at low pressure with 1 bar abs. O_2 pressure (a) and at 130 °C with high pressure 3 bar abs. O_2 (b).

are not sufficiently anchored to the carbon support show a strong tendency to coalesce into large particles [36]. Migration into the ionomer portion of the catalyst layer and coalescence could be predominant with respect to Pt dissolution and reprecipitation [36]. We have observed that the high surface area Ketjenblack carbon produces a better anchoring effect on Pt particles than Vulcan at high temperature as testified by smaller sintering and dissolution phenomena. On the other hand, the effect of cobalt in the PtCo alloy is to decrease the mobility of Pt on carbon; thus, the Ostwald ripening could be predominant in this alloy. It is also worth noting that surface analysis of PtCo/C catalysts has shown an oxide-cleansing action of Co from Pt surface [37]. This characteristic is quite interesting because besides enhancing the catalytic activity for oxygen reduction, due to the removal of strongly adsorbed oxygen species from the Pt surface, addresses the corrosion mechanism mainly towards a dissolution–reprecipitation process. Yu et al. [30] observed that Co dissolution from PtCo catalysts in a MEA at 65 °C did not cause significant performance loss and the membrane conductivity was essentially unchanged.

4. Conclusions

Single cell PEM analysis indicates that significant changes in the Pt electrochemical active surface area may occur after a short period of operation at 130 °C in the presence of humidification constraints. The corresponding variation in the oxygen reduction rate reflects both the actual specific activity and the number of sites available for the reaction. A slight sintering of nanosized Pt particles may produce an increase of performance with respect to the initial characteristics for some catalysts due to the increase in specific activity. Power densities of about 400 mW cm^{-2} at 130 °C were achieved in a PEMFC with 0.3 mg cm^{-2} Pt loading, air feed and Nafion 112 for Pt/C catalysts. A mass activity for oxygen reduction of about 100 A g^{-1} Pt at 130 °C, 0.9 V, air feed (3 bar abs.) has been obtained in the presence of Nafion 112 membrane without correction for hydrogen crossover. The power density increased to about 700 mW cm^{-2} at 130 °C, 0.3 mg cm^{-2} Pt loading, in the presence of oxygen feed (3 bar abs.) and especially with PtCo catalyst.

Degradation test results for the Pt/C catalysts series in sulphuric acid followed a different trend than in PEMFC at 130 °C. At 130 °C, phenomena concerning with Pt sintering, dissolution and precipitation inside the membrane were observed after accelerated tests. The Ketjenblack support appeared to perform better at 130 °C than Vulcan especially in terms of stability at high temperature. However, the characteristics of these carbon supports are still not sufficient to avoid degradation.

Accelerated degradation tests (cycling) showed that all catalysts (Pt and PtCo) are especially affected by significant particle sintering; the particle size increased from two to three times after the tests. However, the degradation mechanism of PtCo appears to be different than that of Pt similarly to what has been shown in low temperature studies [30,31,36]. From the tests carried out in sulphuric acid, it was derived that the carbon corrosion plays the major role on the degradation of the PtCo system. The stability of PtCo in both sulphuric acid and PEM after potential cycling is better than that of Pt/C catalysts. The PtCo catalyst is promising in terms of performance and stability for the high temperature operation. In order to get a further increase in stability for the PtCo system, it would be necessary to replace the Ketjenblack with a more stable support. In this regard, several advancements have been made in the last years [6,32,33]. Among the new supports, particular interest is addressed to carbon nanotubes [32] and Ti suboxides [33]. Hovewer, a highly graphitic and low surface area carbon support could be an appropriate low cost alternative if proper anchoring of the metal particles to the support surface is established. The preparation procedure should be optimised to enhance catalyst dispersion and to obtain a high degree of alloying in conjunction with the new support materials.

Acknowledgement

The authors acknowledge the financial support from European Community through the Autobrane project (FP6).

References

[1] S. Srinivasan, R. Dillon, L. Krishnan, A.S. Aricò, V. Antonucci, A.B. Bocarsly, W.J. Lee, K.-L. Hsueh, C.-C. Lai, A. Peng, Proceedings of the Fuel Cell Science Engineering and Technology, Rochester, 2003, pp. 529–536.

[2] A.S. Aricò, P. Bruce, B. Scrosati, J.-M. Tarascon, W. Van Schalkwijk, Nat. Mater. 4 (5) (2005) 366–377.
[3] H.A. Gasteiger, S.S. Kocha, B. Sompalli, F.T. Wagner, Appl. Catal. B: Environ. 56 (2005) 9–35.
[4] C. Jaffray, G.A. Hards, in: W. Vielstich, A. Lamm, H. Gasteiger (Eds.), Handbook of Fuel Cells—Fundamentals, Technology and Applications, vol. 3, Wiley, Chichester, UK, 2003, p. 509 (Chapter 41).
[5] T. Tada, in: W. Vielstich, A. Lamm, H. Gasteiger (Eds.), Handbook of Fuel Cells—Fundamentals, Technology and Applications, vol. 3, Wiley, 2003, p. 481 (Chapter 38).
[6] R. Atanasoski, Proceedings of the 4th International Conference on Applications of Conducting Polymers, ICCP-4, Como, Italy, February 18–20, 2004.
[7] J. Scholta, N. Berg, P. Wilde, L. Jörissen, J. Garche, J. Power Sources 127 (2004) 206–212.
[8] A.S. Aricò, P.L. Antonucci, V. Antonucci, in: A. Wieckowski, E.R. Savinova, C.G. Vayenas (Eds.), Catalysis and Electrocatalysis at Nanoparticle Surfaces, Marcel Dekker, Inc., New York, 2003.
[9] G. Alberti, M. Casciola, Annu. Rev. Mater. Res. 33 (2003) 129–154.
[10] A.S. Aricò, V. Baglio, A. Di Blasi, P. Cretì, P.L. Antonucci, V. Antonucci, Solid State Ionics 161 (2003) 251–265.
[11] K.D. Kreuer, Solid State Ionics 97 (1997) 1–15.
[12] S. Reichman, T. Duvdevani, A. Aharon, M. Philosoph, D. Golodnitsky, E. Peled, J. Power Sources 153 (2006) 228–233.
[13] O. Savadogo, J. New Mater. Electrochem. Syst. 1 (1998) 47–66.
[14] N. Giordano, P.L. Antonucci, E. Passalacqua, L. Pino, A.S. Aricò, K. Kinoshita, Electrochim. Acta 36 (1991) 1931–1935.
[15] Q. Li, R. He, J.O. Jensen, N.J. Bjerrum, Chem. Mater. 15 (2003) 4896–4915.
[16] K. Kinoshita, Electrochemical Oxygen Technology, Wiley, New York, 1992.
[17] N. Giordano, E. Passalacqua, L. Pino, A.S. Aricò, V. Antonucci, M. Vivaldi, K. Kinoshita, Electrochim. Acta 36 (1991) 1979–1984.
[18] N.M. Markovic, T.J. Schmidt, V. Stamenkovic, P.N. Ross, Fuel Cells: Fundam. Syst. 1 (2001) 105.
[19] S. Mukerjee, S. Srinivasan, in: W. Vielstich, A. Lamm, H. Gasteiger (Eds.), Handbook of Fuel Cells—Fundamentals, Technology and Applications, vol. 2, Wiley, Chichester, UK, 2003, p. 502 (Chapter 34).
[20] A.S. Aricò, V. Baglio, A. Di Blasi, E. Modica, P.L. Antonucci, V. Antonucci, J. Electroanal. Chem. 557 (2003) 167–176.
[21] A.S. Aricò, A.K. Shukla, K.M. El-Khatib, P. Cretì, V. Antonucci, J. Appl. Electrochem. 29 (1999) 671–676.
[22] E. Antolini, J.R.C. Salgado, E.R. Gonzalez, J. Power Sources 160 (2006) 957–968.
[23] V. Stamenkovic, T.J. Schmidt, P.N. Ross, N.M. Markovic, J. Phys. Chem. B 106 (2002) 11970–11979.
[24] N.M. Markovic, P.N. Ross, Surf. Sci. Rep. 45 (2002) 117–125.
[25] O. Antoine, Y. Bultel, R. Durand, J. Electroanal. Chem. 499 (2001) 85–94.
[26] D. Thompsett, in: W. Vielstich, H. Gasteiger, A. Lamm (Eds.), Handbook of Fuel Cells—Fundamentals, Technology and Applications, vol. 3, Wiley, Chichester, UK, 2003, p. 467 (Chapter 37).
[27] S.C. Ball, S.L. Hudson, D. Thompsett, B. Theobald, J. Power Sources 171 (2007) 18–25.
[28] M. Cai, M.S. Ruthkosky, B. Merzougui, S. Swathirajan, M.P. Balogh, J. Power Sources 160 (2006) 977–986.
[29] N. Giordano, P.L. Antonucci, E. Passalacqua, L. Pino, A.S. Aricò, K. Kinoshita, Electrochem. Acta 36 (13) (1991) 1931–1935.
[30] P. Yu, M. Pemberton, P. Plasse, J. Power Sources 144 (2005) 11–20.
[31] H.R. Colón-Mercado, B.N. Popov, J. Power Sources 155 (2006) 253–263.
[32] X. Wang, W. Li, Z. Chen, M. Waje, Y. Yan, J. Power Sources 158 (2006) 154–159.
[33] T. Ioroi, Z. Siroma, N. Fujiwara, S. Yamazaki, K. Yasuda, Electrochem. Commun. 7 (2005) 183–188.
[34] S.S. Kocha, in: W. Vielstich, A. Lamm, H. Gasteiger (Eds.), Handbook of Fuel Cells—Fundamentals, Technology and Applications, vol. 3, Wiley, Chichester, UK, 2003, p. 538 (Chapter 43).
[35] K. Yasuda, A. Taniguchi, T. Akita, T. Ioroi, Z. Siroma, J. Electrochem. Soc. 153 (8) (2006) A1599–A1603.
[36] R.L. Borup, J.R. Davey, F.H. Garzon, D.L. Wood, M.A. Inbody, J. Power Sources 163 (2006) 76–81.
[37] A.S. Aricò, A.K. Shukla, H. Kim, S. Park, M. Min, V. Antonucci, Appl. Surf. Sci. 172 (2001) 33–40.